Accepted Manuscript

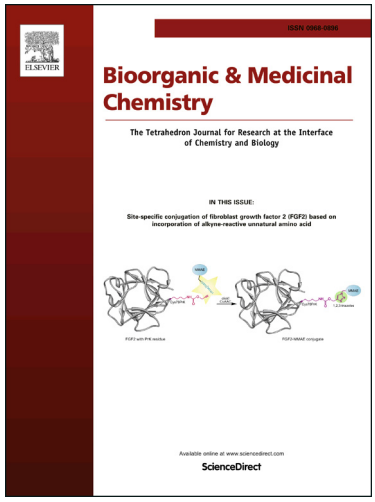

Platinum(IV) complexes conjugated with phenstatin analogue as inhibitors of microtubule polymerization and reverser of multidrug resistance

Xiaochao Huang, Rizhen Huang, Shaohua Gou, Zhimei Wang, Zhixin Liao, Hengshan Wang

PII: S0968-0896(17)31089-1
DOI: http://dx.doi.org/10.1016/j.bmc.2017.07.011
Reference: BMC 13847

To appear in: *Bioorganic & Medicinal Chemistry*

Received Date: 18 May 2017
Revised Date: 4 July 2017
Accepted Date: 6 July 2017

Please cite this article as: Huang, X., Huang, R., Gou, S., Wang, Z., Liao, Z., Wang, H., Platinum(IV) complexes conjugated with phenstatin analogue as inhibitors of microtubule polymerization and reverser of multidrug resistance, *Bioorganic & Medicinal Chemistry* (2017), doi: http://dx.doi.org/10.1016/j.bmc.2017.07.011

Platinum(IV) complexes conjugated with phenstatin analogue as inhibitors of microtubule polymerization and reverser of multidrug resistance

Xiaochao Huang, [a, b, 1] Rizhen Huang, [a, b, 1] Shaohua Gou,[a, b, *] Zhimei Wang,[a, b] Zhixin Liao [a , b] and Hengshan Wang [c,*]

[a] Pharmaceutical Research Center and School of Chemistry and Chemical Engineering and [b] Jiangsu Province Hi-Tech Key Laboratory for Biomedical Research, Southeast University, Nanjing 211189, China.

[c] State Key Laboratory for the Chemistry and Molecular Engineering of Medicinal Resources (Ministry of Education of China), School of Chemistry and Pharmaceutical Sciences of Guangxi Normal University, Guilin 541004, China.

ABSTRACT: Pt(IV) complexes comprising a phenstatin analogue, as dual-targeting Pt(IV) prodrug, were designed and synthesized. They were found not only to carry the DNA binding platinum warhead into the tumor cells, but also to have a small molecular unit to inhibit tubulin polymerization. *In vitro* evaluation results revealed that Pt(IV) complexes showed better and more potent activity against the test human cancer cells including cisplatin resistant cell lines than their corresponding Pt(II) counterparts. In addition, the Pt(IV) derivative of cisplatin, complex **10**, exhibited highly selective inhibition in human cancer cells and displayed no obvious toxicity to two human normal cell lines, respectively. Mechanism study suggested that complex **10** induced cell-cycle arrest at the G2/M phase and caused apoptotic cell death of human lung cancer NCI-H460 cells through the mitochondrial mediated pathway. Moreover, complex **10** effectively inhibited the tumor growth in the NCI-H460 xenograft model.

Keywords: Antitumor activity; Pt(IV) complex; Tubulin polymerization; Apoptosis

* Corresponding author.

Corresponding author: E-mail addresses: sgou@seu.edu.cn (S. Gou), whengshan@163.com (H. -S. Wang). [1] Co-first author: These authors contributed equally to this work.

1. Introduction

Cisplatin (**Fig. 1**), representing one of the most powerful anticancer drugs, has been widely used for the treatment of a variety of cancers since it was approved for clinical use in 1978.[1-4] Although cisplatin is effective, the side effects including nephrotoxicity, neurotoxicity and toxicity have largely limited its clinical applications.[5-8] In addition, drug resistance, both inherent and acquired, is another important reason for treatment failure of Pt(II) drugs.[9-11] Thus, the development of novel and more effective platinum based drugs to overcome the shortcomings of cisplatin is still an important issue of today's research.

Recent studies indicated that combination of platinum anticancer agents with tubulin inhibitors including paclitaxel and docetaxel can lead to the improvement of chemotherapeutic efficacy.[12] Up to now, the natural products including vincristine, paclitaxel, vinblastine, combretastatin-A 4 and docetaxel, as inhibitor of tubulin, are forceful as anti-mitotic drugs that can effectively induce tumor cell apoptosis and obviously inhibit tumor cell proliferation and angiogenesis.[13] Microtubules are cytoskeletal filaments comprising α- and β-tubulin that polymerise parallel to a cylindrical axis.[14] Microtubules, which plays an important role in cellular processes involved in the formation of the mitotic spindle, cell proliferation, intracellular transport and cell signaling, have been considered as a fascinating molecular target for antitumor agents in recent years.[15-17] Anti-mitotic agents attack microtubules by interfering with the dynamics of tubulin polymerization or dissociation, leading to mitotic arrest.[18] So far two major types of antitumor drugs have presented their effectiveness in this mechanism, defined as microtubule stabilizing agents (e.g. paclitaxel, discodermolide) and microtubule destabilizing agents (e.g. vinca alkaloids, colchicine and combretastatin-4).[19, 20] Combretastatin-A 4 (CA-4, **Fig. 2**) as a natural cis-stilbene product, isolated by Pettit and co-workers in 1988 from the bark of African willow tree *Combretum caffrum*, was found to inhibit strong tubulin polymerization by binding to the colchicine binding site.[21, 22] Besides, CA-4 has been known to exert potent cytotoxicity against a large number of human cancer cells including multidrug resistant ones.[23-27]

It is generally considered that CA-4 has three major pharmacophone components: two hydrophobic rings (rings A and B) and a linking bridge between the aromatic rings.[18] Research on CA-4 to increase its *in vivo* activity has led to the discovery of phenstatin (**Fig. 3**). Phenstatin, a

benzophenone type CA-4 analogue, synthesized by Pettit's group with a carbonyl moiety in place of an ethylene (CH_2=CH_2) bridge between the two rings, was studied to be a tubulin polymerization inhibitor which binded to the colchicine site and exhibited potent cytotoxicity against a variety of human cancer cells including multidrug resistant cancer cell lines.[28-30] Particularly, Schobert and co-workers reported that the Pt(II) complexes conjugating with chalcone exhibited moderate anti-proliferative activities, due to the different mode of actions such as DNA-targeting Pt(II) complexes and tubulin-targeting chalcone moieties.[31] Therefore, a combination of cytotoxic DNA damaging platinum-based drugs with tubulin inhibitors can be an attractive strategy for targeting microtubules and DNA, and at least in theory, can improve the anticancer activity of platinum drugs and overcome their adverse side effects. Pt(IV) complexes as prodrugs, showing kinetic inertness compared with their Pt(II) counterparts, are expected to exhibit great promise in the search for the next generation of platinum drugs, because they can be effectively reduced to Pt(II) equivalents once inside the cells. Recently, there have been several reports about Pt(IV) prodrugs conjugated with phenylbutyrate, chalcone derivatives or dichloroacetate as the axial ligands in the octahedral geometry of Pt(IV) complexes, in which Pt(IV) species were easily reduced to their Pt(II) equivalents inside the tumor cells in the presence of ascorbic acid or glutathione and released other molecular fragments to activate p53, inhibit histone deacetylases (HDACs), suppress efficacy of pyruvate dehydrogenase kinase (PDK) and induce cell cycle arrest at the S and G2/M phases and cell death through apoptosis, respectively.[32-39]

In our previous work, we reported three Pt(IV) complexes containing a CA-4 analogue as dual-targeting Pt(IV) prodrug. Among them, the Pt(IV) derivative of cisplatin comprising a CA-4 analogue displayed potent antitumor activities against the test cancer cell lines and effectively inhibit the tumor growth in the HepG-2 xenograft model.[40] However, the *in vivo* activity of the reported complex was lower than that of cisplatin. In order to search for novel Pt(IV) complex prodrugs with higher antitumor activities against the human cancer lines and lower toxicity toward human normal cells, dual-targeting Pt(IV) complexes containing a phenstatin analogue were studied herein as anticancer prodrugs with the ability to release Pt(II) equivalents and the phenstatin analogue for their respective biological actions. Apart from their effective *in vitro* anti-proliferative activities, *in vivo* tumor inhibition of a representative Pt(IV) complex together

with its mechanism of apoptotic pathway was also investigated.

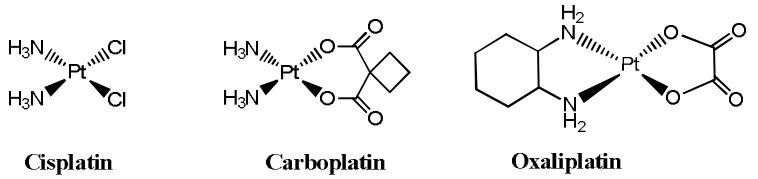

Fig. 1. FDA approved Pt(II) anticancer agents.

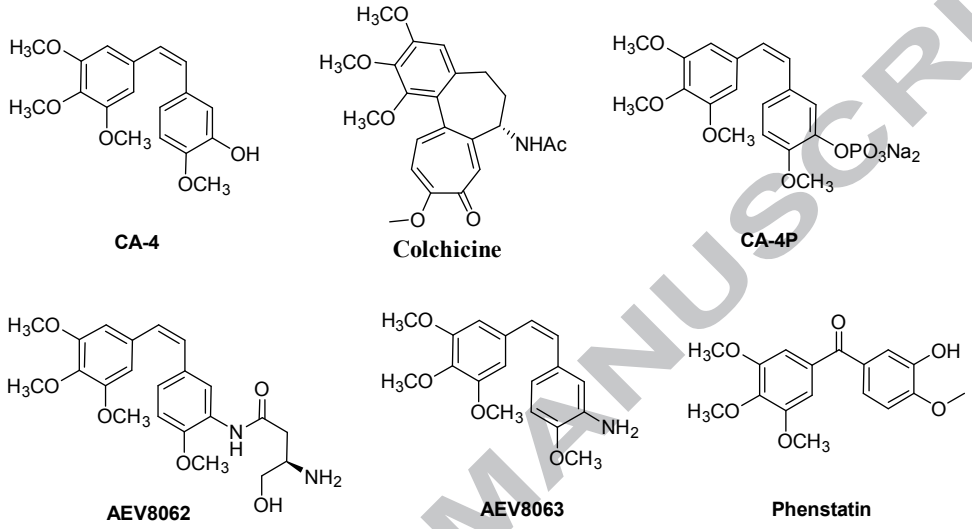

Fig. 2. Chemical structures of natural products and clinical trial agents that bind at the colchicine-binding site of tubulin.

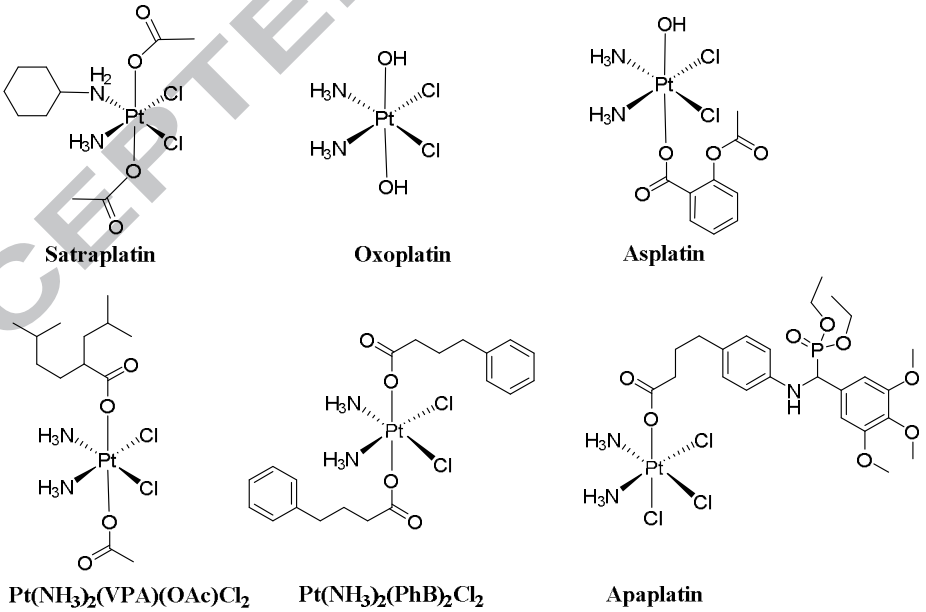

Fig. 3. Chemical structures of a few Pt(IV) prodrugs

2. Results and discussion

2.1 Design and synthesis.

Compounds **1-4** were synthesized according to the reported procedures.[41] Pt(IV) complexes **7-9** were prepared in agreement with the literature method.[42] Compound **4** upon etherification with α-bromoethyl acetate, K_2CO_3 and KI in the presence of DMF gave ester **5** followed by its hydrolysis with aluminum hydroxide to afford the acid **6**. The synthesis of target compounds was achieved by the formation of ester bond between **6** and Pt(IV) complexes **7-9**, respectively, in the presence of TBTU/Et_3N. The target compounds were characterized by microanalysis, ^{1}H, and ^{13}C NMR spectra together with HR-MS spectrometry. The synthetic profiles of the compounds and their chemical structures are listed in **Scheme 1**.

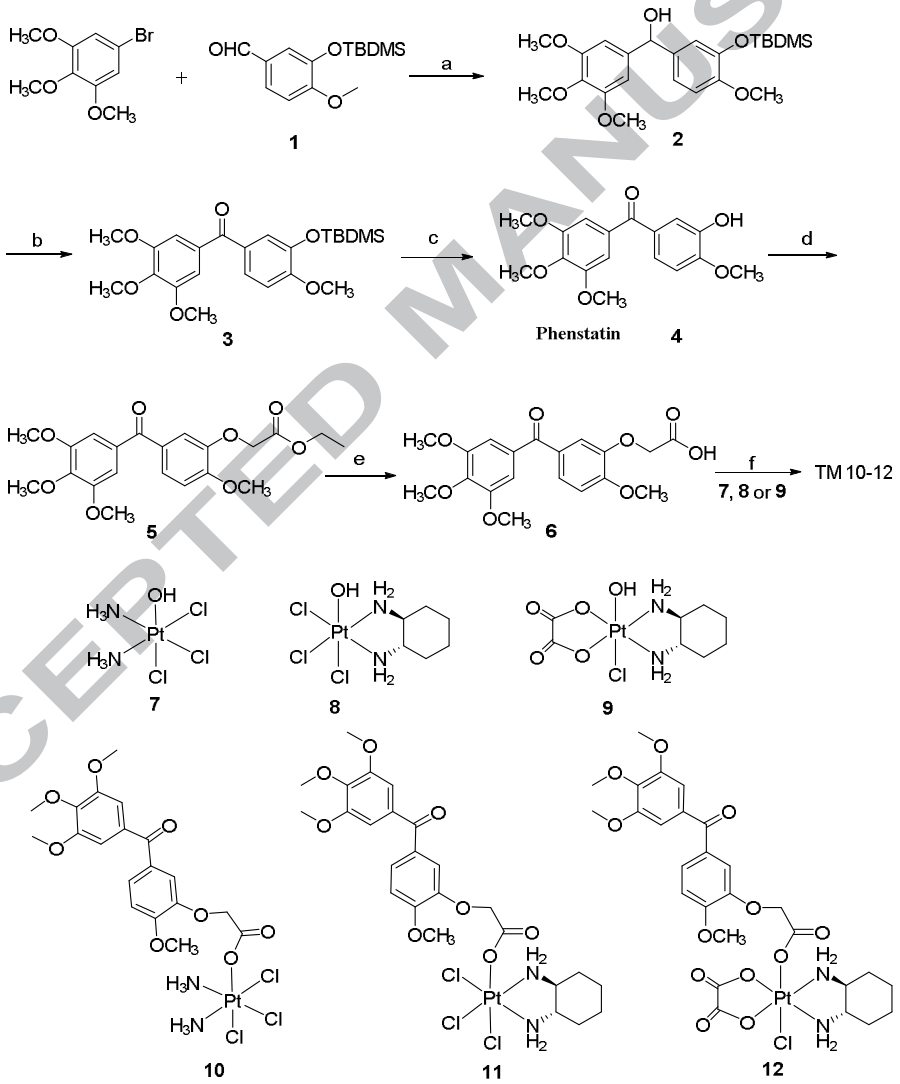

Scheme 1. Synthetic Pathway to Prepare Target Compounds **10-12**. Reagents and Conditions: (a)THF, n-BuLi, -78 ^{o}C; (b) PDC, CH_2Cl_2, rt; (c) 1N HCl/CH_3OH, 50 ^{o}C; (d) K_2CO_3, DMF, rt.; (e)

$LiOH.H_2O$, THF/H_2O, rt.; (f) TBTU, Et_3N, DMF, rt.

2.2. HPLC analyses on the released ability of the resulting Pt(IV) complexes.

To evaluate whether our Pt(IV) complexes can be reduced to their Pt(II) equivalents or not, complex **10** in a solution of acetonitrile and water (1.5:1) to release compound **6** and cisplatin in the presence of ascorbic acid was examined by HPLC. As illustrated in **Fig. S1**, complex **10** gradually released compound **6** as time passed, accompanied by the falling down peak of complex **10** and the rising peak of compound **6**, respectively. It was found in the HPLC chromatograms that cisplatin was not observed due to its weak chromophore in the ultraviolet detecting condition. Under the same condition, the behavior of complex **12** was also examined for comparison, because oxaliplatin could be observed in HPLC chromatograms. As shown in **Fig. S1**, similar results for complex **12** were observed in HPLC chromatograms except the presence of oxaliplatin. Taken together, these data demonstrated that the Pt(IV) complexes were easily reduced to their Pt(II) equivalents under the ascorbic acid at the room temperature, releasing the corresponding active drug species.

2.3 In vitro cytotoxicity assay.

The *in vitro* cytotoxicity of the target Pt(IV) complexes **10-12** were investigated using MTT assay on a panel of human cancer cell lines including HepG-2 (hepatoma), Bel-7404 (hepatoma), NCI-H460 (lung), MGC-803 (gastric), and human normal cell lines such as HL-7702 (human normal liver cell line) and NCM460 (human normal colon mucosal epithelial cell line). Phenstatin, CDDP, OXP and DACHPt were used as the positive controls. The corresponding IC_{50} values, obtained after 72 h exposure, are given in Table 1. *In vitro* evaluation results revealed that phenstatin analogue **6** exhibited lower cytotoxicity against the tested tumor cell lines than phenstatin. However, complexes **10-12**, the Pt(IV) derivative of cisplatin, oxaliplatin, or DACHPt with one phenstatin analogue ligand in the axial position, possessed higher cytotoxicity against all test cancer cell lines than the positive control. Especially, complex **10**, the Pt(IV) derivative of cisplatin with one phenstatin analogue ligand in the axial position, possessed better antitumor activities against all test cancer cell lines than that of cisplatin, with IC_{50} values in the range of 0.55–1.97 μM, and synchronously displayed lower cytotoxicity toward NCM460 and HL-7702 with IC_{50} values of 35.13±2.41 and 45.03±2.55 μM than cisplatin (15.21±0.35 and 6.30±0.32 μM)

and phenstatin (2.01±0.54 and 1.41±0.16 μM), respectively. Pt(IV) complexes **11** and **12** also exhibited better anti-proliferative activity against the tested cell lines than their corresponding Pt(II) counterparts, DACHPt and oxaliplatin, with IC_{50} values in the range of 0.61–1.30 and 0.98–4.07 μM, respectively. Interestingly, complex **10** exhibited up to 7.7-fold increased cytotoxicity compared with cisplatin in HepG-2 cells and showed significantly more effective anticancer activity than phenstatin. The similar trend was also observed in Bel-7404 and NCI-H460 cells. Notably, all Pt(IV) complexes revealed lower cytotoxicity than their corresponding positive references (CDDP, OXP and DACHPt) against two human normal cell lines, indicating that these complexes have a selective toxicity for the cancer cells over the normal cell.

Table 1. Biological activity of Pt(IV) complexes **10-12**.

Compd.	IC_{50} (μM) [d]					
	HepG-2	Bel-7404	NCI-H460	MGC-803	NCM460	HL-7702
6	19.82±1.27	25.37±2.03	10.21±2.03	25.54±2.35	55.23±3.02	65.27±2.19
10	0.62±0.04	1.97±0.45	0.55±0.06	0.64±0.11	35.13±2.41	45.03±2.55
11	0.78±0.07	1.30±0.22	0.91±0.21	0.61±0.18	37.42±1.58	37.42±2.59
12	2.08±0.28	4.07±0.39	1.75±0.33	0.98±0.20	39.63±3.27	49.63±2.01
Phenstatin	0.69±0.05	2.25±0.57	0.70±0.16	0.31±0.08	2.01±0.54	1.41±0.16
CDDP [a]	4.76±0.41	4.38±0.52	3.21±0.42	6.90±0.75	15.21±2.35	6.30±0.32
OXP [b]	5.06±0.20	7.90±0.71	4.23±0.39	5.24±0.31	16.52±0.93	8.23±0.52
DACHPt [c]	4.06±0.17	6.21±0.32	3.51±0.42	4.49±0.14	13.65±1.04	5.65±0.74

[a] Cisplatin, [b] Oxaliplatin, [c] Dichloro(1*R*,2*R*-diaminocyclohexane)platinum(II). [d] IC_{50} is the drug concentration effective in introducing 50% of cell death measured by MTT assay after 72 h drug exposure and mean values ± standard deviation depend on three independent experiments.

2.4. Antitumor activity against cisplatin resistant cell lines.

According to the above biological result, we further investigated sensitivity of the Pt(IV) complexes (**10-12**) against cisplatin resistant and the corresponding normal cancer cells (human ovarian cancer cell SK-OV-3, human lung epithelial cell A549). As shown in Table 2, the IC_{50} value of cisplatin toward SK-OV-3 and A549 resistant cell lines were increased to 15.61 and 29.05 μM, respectively, compared with those of cisplatin toward the normal cancer cell lines.

Interestingly, the activity of complex **10** did not significantly vary for both these two cisplatin resistant cancer cell lines and the non-resistant ones. Its IC_{50} values toward cisplatin resistant SK-OV-3 and A549 cell lines were 1.41 and 1.95 μM, respectively. Notably, complex **10** had a much lower resistance index (1.88 for resistant SK-OV-3 cells and 1.93 for resistant A549 cells) than cisplatin (18.15 for resistant SK-OV-3 cells and 6.92 for resistant A549 cells). The similar tendency was also observed in complexes **11** and **12**, suggesting that these complexes might be effective in the treatment of drug refractory tumors resistant to other Pt(II) drugs.

Table 2. *In vitro* growth inhibitory effect of Pt(IV) complexes on cisplatin-resistant cancer cells.

Compd.	IC_{50} (μM)		resistant	IC_{50} (μM)		resistant
	SK-OV-3	SK-OV-3/CDDP	factor [d]	A549	A549/CDDP	factor [d]
6	12.11±0.95	21.32±2.13	1.76	26.16±2.13	32.11±2.07	1.22
10	0.75±1.09	1.41±0.19	1.88	1.01±0.24	1.95±0.12	1.93
11	0.95±0.12	1.72±0.21	1.81	1.25±0.37	1.86±0.19	1.49
12	2.63±0.49	3.53±2.59	1.34	1.86±0.68	2.67±0.66	1.44
Phenstatin	0.86±0.31	1.61±0.46	1.87	3.26±0.33	5.66±0.77	1.74
CDDP [a]	0.86±0.31	15.61±0.46	18.15	4.20±0.61	29.05±1.55	6.92
OXP [b]	5.61±0.25	16.21±2.31	2.88	5.36±0.70	23.21±2.01	4.33
DACHPt [c]	4.12±0.38	17.04±1.55	4.41	5.21±0.47	19.54±0.32	3.75

[a] Cisplatin, [b] Oxaliplatin, [c] Dichloro(1*R*,2*R*-diaminocyclohexane)platinum(II), [d] The values express the ratio between IC_{50} determined in resistant and nonresistant cell lines.

2.5. Cell uptake and cell viability.

Since complex **10** showed potent anti-proliferative effects, it was selected to carry out the cellular uptake test in NCI-H460 cells by using the inductively coupled plasma mass spectrometry (ICP-MS). As shown in **Fig. 4** A and Table 3, treating NCI-H460 cells with complex **10** (5.0 and 10.0 μM) for 24 h resulted in a substantial increase in the content of cellular platinum in a dose dependent manner, suggesting facile internalization of complex **10** within 24 h. Especially, the uptake of this complex was remarkably higher than those of cisplatin. After exposure to 10.0 μM of complex **10** for 24 h, the concentration of cellular platinum rose to 459 ng/10^6 cells, which is nearly up to 2.1 times as much as that of cisplatin. According to the corresponding experimental

results from the cytotoxicity assay and cellular uptake tests, it seems that the improvement of cellular uptake can result in the increase of the antitumor activity.

The effect of complex **10** on cell proliferation after 72 h treatment was further assessed in NCI-H460 cancer cell line using MTT assay. Our results found that the complex **10** was significantly inhibited cell proliferation in human lung cancer cells compared with cisplatin under the same conditions (**Fig. 4** B).

Table 3. Cellular uptake of complex **10** in NCI-H460 cells.

Complex	Pt content (ng/10^6 cells) [b]
	NCI-H460
10 (5 μM)	175±20
10 (10 μM)	459±46
CDDP (5 μM)	105±12
CDDP (10 μM)	219±22

[a] Cisplatin. [b] Incubation for 24 h. Results are expressed as the mean ± SD for three independent experiments.

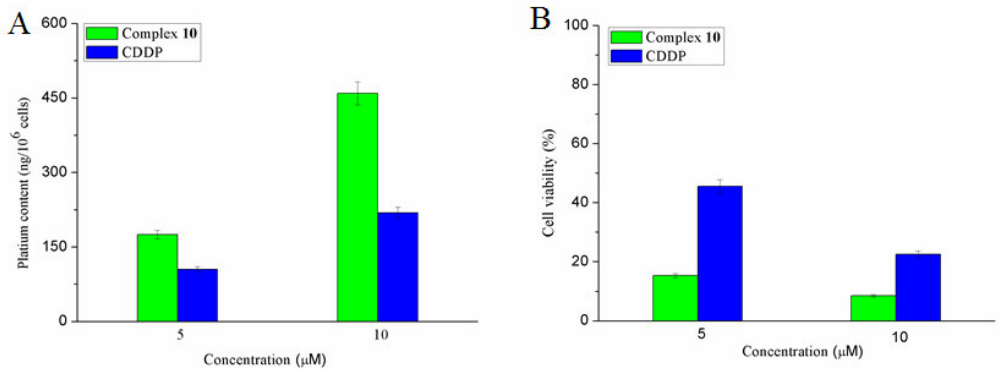

Fig. 4. (A) Intracellular accumulation of complex **10**, and CDDP (5, 10μM) in NCI-H460 cells after 24 h. Each value is in nanograms of platinum per10^6 cells. (B) *In vitro* cytotoxicity of complex **10**, and CDDP toward NCI-H460 cancer cells at the same concentration for 72 h. Results are expressed as the mean ± SD of three independent experiments. $P < 0.05$

2.6. Competitive binding to colchicine binding site of tubulin.

Compounds **6**, **10**, phenstatin and CA-4 were examined for inhibitory effects on tubulin polymerization and for binding effects on [^{3}H] colchicine to tubulin in determining whether their antitumor effects might be caused by an interaction with microtubules. For comparison, CA-4 and

phenstatin were evaluated in contemporaneous experiments. The result is given in Table 4. In the colchicine binding studies, both **6** and **10** are capable of inhibiting tubulin polymerization with calculated IC_{50} values of 12.5 μM and 13.9 μM, respectively. In addition, **10** showed the ability to compete with [^{3}H] colchicine in binding to tubulin. The binding potency of **10** (42.5%) to the tubulin colchicine binding site, comparable to **6** (45.0%), was much stronger than that of cisplatin but less than that of CA-4 (98%) and phenstatin (99%), respectively.

Table 4. Inhibition of tubulin polymerization and colchicine binding by complexes **6**, **10**, CDDP, CA-4 and Phenstatin.

Compd. (10 μM)	Tubilin assembly [a] IC_{50} (μM)	Colchicines binding [b] (% inhibition)
6	12.5±1.3	45.0±1.2
10	13.9±1.5	42.5±1.3
CDDP [c]	>100	<5
CA-4	1.1±0.2	98.0±0.5
Phenstatin	0.6±0.3	99.0±0.3

[a] Inhibition of tubulin polymerization. Tubulin was at 10 μM. [b] Inhibition of [^{3}H] colchicine binding. Tubulin, colchicine and the tested compound were at 1, 5, and 5 μM, respectively. [c] Cisplatin.

*2.7 Complex **10** inhibited the polymerization of tubulin in vitro.*

It is generally known that the mechanism of tubulin-binding agents can be divided into two types: stimulating agents and inhibiting agents.[20] In order to determine which type complex **10** belongs to, its effect on the assembly kinetics of tubulin with paclitaxel, CA-4 and phenstatin as references was evaluated. As illustrated in **Fig. 5**, paclitaxel (10 μM) was found to stimulate tubulin polymerization, while CA-4 (10 μM) or phenstatin (10 μM) almost inhibited tubulin polymerization as expected. For complex **10**, an obvious inhibition of polymerization was observed at two concentrations, and the rate of assembly as well as the final amount of microtubules was lower than the control group.

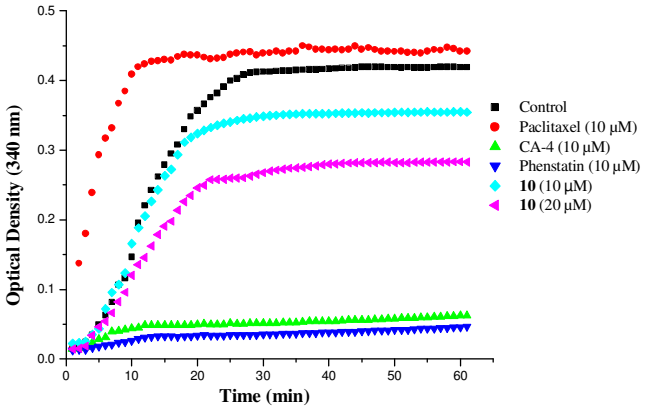

Fig. 5. Effects of complex **10** on microtubule dynamics. Polymerization of tubulin at 37 °C in the presence of paclitaxel (10 μM), CA-4 (10 μM), phenstatin (10 μM) and complex **10** (10 μM and 20 μM) were monitored continuously by recording the absorbance at 340 nm over 60 min. The reaction was initiated by the addition of tubulin to a final concentration of 3.0 mg/mL.

2.8. Molecular modeling.

To determine the possible binding mode of the Pt(IV) complexes, compounds **6** and **10** were chosen to perform a molecular docking to ensure that the Pt(IV) complexes have the same binding site as colchicine and CA-4. The binding modes of compounds **6** and **10** in the colchicine binding site of tubulin are depicted in **Fig. 6**. The Surflex docking scores are 12.06 for **10** and 8.57 for **6**, where higher scores indicate greater binding affinity (data not shown). Biological activity studies suggested that complex **10** potentially inhibited tubulin polymerization, hence, the docking detail of complex **10** was examined to compare with those of 3E22-colchicine and CA-4 to evaluate binding modes.

Fig. 6 C and D show that the interacting mode of CA-4 with 3,4,5-trimethoxyphenyl rings in the binding site is surrounded by Ser178, Ala180, Ala316, Val315, Asn350, Lys352, Phe377 and Gly379. In particular, CA-4 forms three hydrogen bonds with the polar amino acids Asn249, Ala 250 and Asn258, suggesting a probable strong electrostatic interaction with the protein. In addition, the hydrophobic moiety of the 3E22-colchicine is well embedded in a pocket interacting with several hydrophobic residues making 3E22-colchicine bind tightly to tubulin. Not surprisingly, the accommodation of compound **6** in the binding site is similar to colchicine (**Fig. 6 F**). Also in this case, docking simulations showed that the 3,4,5-trimethoxy-phenyl rings of

compound **6** like colchicine can also be accommodated in the same hydrophobic groove, adopting an energetically stable conformation. Moreover, the methoxy group in compound **6** as an acceptor establishes three hydrogen bonds with Asn101, Asn249 and ALA250, which is consistent with the observation that colchicine stabilizes the tubulin heterodimer and further confirms that this moiety is also crucial for binding (**Fig. 6** A and B). As shown in **Fig. 6** E, in comparison with CA-4 or colchicine, complex **10** inserts a deep cave and formed hydrogen bonding with VAL315 and ASN350, respectively. In addition, the 3,4,5-trimethoxy-phenyl ring of complex **10** also establishes three hydrogen bonds with ASN101, ASN249 and ALA250, which is similar to CA-4 and compound **6**. It is interesting to note that the crucial electrostatic interactions between the methoxy group of the 3,4,5-trimethoxy-phenyl unit and residues Ser178 and Asn101 of the neighboring α-subunit were observed in the binding pocket, demonstrating a plausible competitive mechanism of action at the colchicine site.

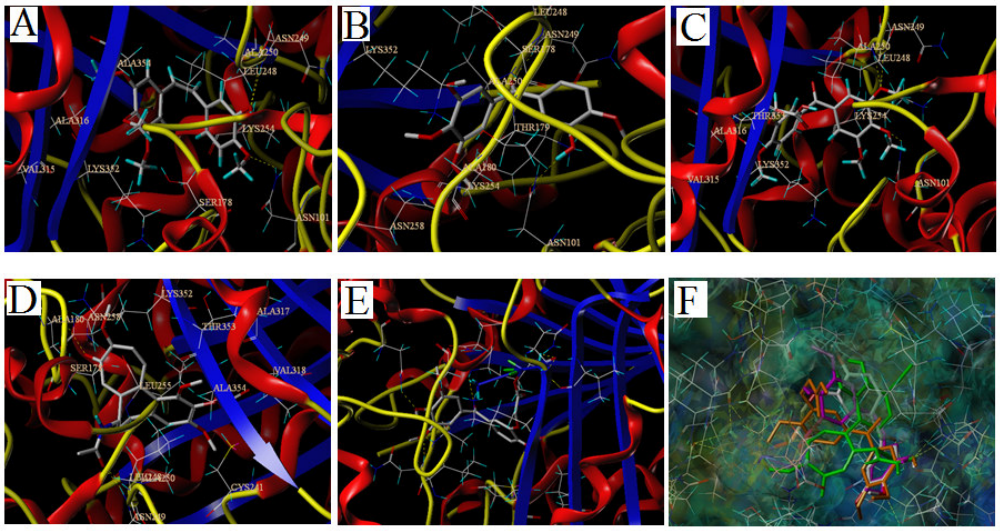

Fig. 6. Molecular modeling of CA-4, phenstatin, 3E22-colchicine and compound **6** in complex with tubulin. Illustrated are the proposed binding mode and interaction between tubulin and selected compounds, (A) CA-4, (B) phenstatin, (C) compound **6**, (D) 3E22-colchicine, (E) complex **10**. (F) Comparison of the crystallographic structure of colchicines (in green), CA-4 (in purple), compound **6** (in orange) in complex with tubulin (Protein Data Bank Code 3E22) and the energetically most favorable pose of complex **10** (in gray) obtained by molecular docking simulation. Hydrogen atoms are omitted.

2.9. Effect on cell cycle arrest.

To evaluate the effect of the synthetic compound **10** on cell cycle arrest, we used flow cytometry to examine the cell cycle distribution of NCI-H460 cells following a 24 h treatment with complex **10** at different concentrations. Untreated cells were used as a negative control, and cells treated with cisplatin were used as a positive control. It is noted from **Fig. 7** A that in the G2 phase, the percentage of cells treated with complex **10** increased to 30.30% (5 μM) and 65.87% (10 μM) compared with the control. But cells treated with cisplatin 10 μM for 24 h, the percentage of cells in the S phase increased to 35.23% compared with untreated cells. These results showed that complex **10** may cause cell accumulation in the G2 phase of the cell cycle by either delaying or inhibiting progression to the next phase.

Furthermore, the association between the induced G2 arrest by complex **10** and alterations in expression of various proteins that regulate cell division were evaluated. Cyclin B in its complex with CDK1, which triggers entry into mitosis, is considered to be a major regulator of G2/M checkpoint.[43, 44] Protein p53 and p21 play a key role in G2 arrest through accumulation of inactive cyclin B1/p34^{cdc2} complex.[45-47] Thus, the levels of regulatory proteins implicated in G2 arrest, including p21, p53, CDK1 and cyclin B1, were investigated. As shown in **Fig. 7** B, the expression of CDK1 and Cyclin B1 were significantly down-regulated, but p21 and p53 levels were significantly up-regulated in NCI-H460 cells after complex **10** treatment. These results suggesting that the cells are effectively arrested at G2 phase of the cell cycle.

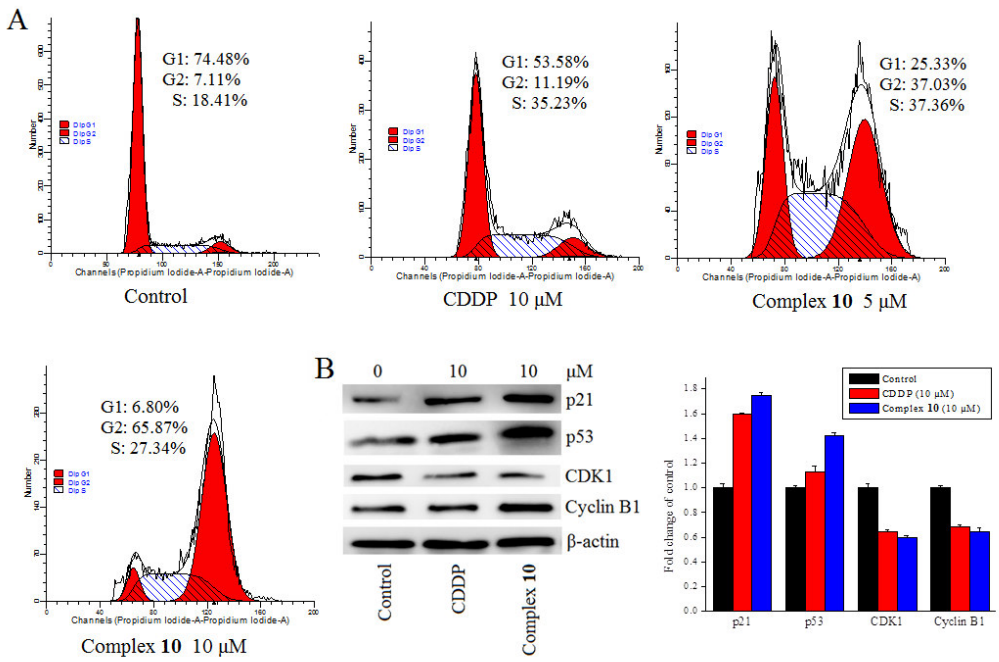

Fig. 7. (A) Investigation of cell cycle distribution by flow cytometry analysis. Untreated NCI-H460 cells as a control. NCI-H460 cells were treated with complex **10** (5 and 10 μM) and CDDP (10 μM) as positive control for 24 h, respectively. (B) Western blot analysis of p21, p53, CDK1 and Cyclin B1 in NCI-H460 cells treated with complex **10** (10 μM) for 48 h. CDDP (10 μM) was used as a positive control, β-actin was used as the internal control. Data are expressed as the mean ± SEM of three independent experiments.

*2.10. Complex **10** induced apoptotic cell death.*

The mode of cell death induced by complex **10** was investigated with the annexin-V/propidium iodide (PI) assay and the number of apoptotic cells was evaluated by flow cytometry. NCI-H460 cells were treated with complex **10** with cisplatin served as a positive control. Q1, Q2, Q3, and Q4 represent four different cell states: necrotic cells, late apoptotic or necrotic cells, apoptotic cells and living cells, respectively. A dose-dependent improvement in the percentage of apoptotic cells was evident after the cells were treated with complex **10** for 24 h at the concentrations of 5 μM and 10 μM, respectively. As shown in **Fig. 8**, the percentage of cell apoptosis was 6.51% for the control, and cell apoptosis was added up to 10.36% and 26.5% at 5 and 10 μM of cisplatin; while treated with complex **10** at 5 and 10 μM, the percentage of cell apoptosis was increased to 17.59% and 69.8%, respectively. Taken together, the results clearly demonstrated that complex **10** effectively induced apoptosis in NCI-H460 cells.

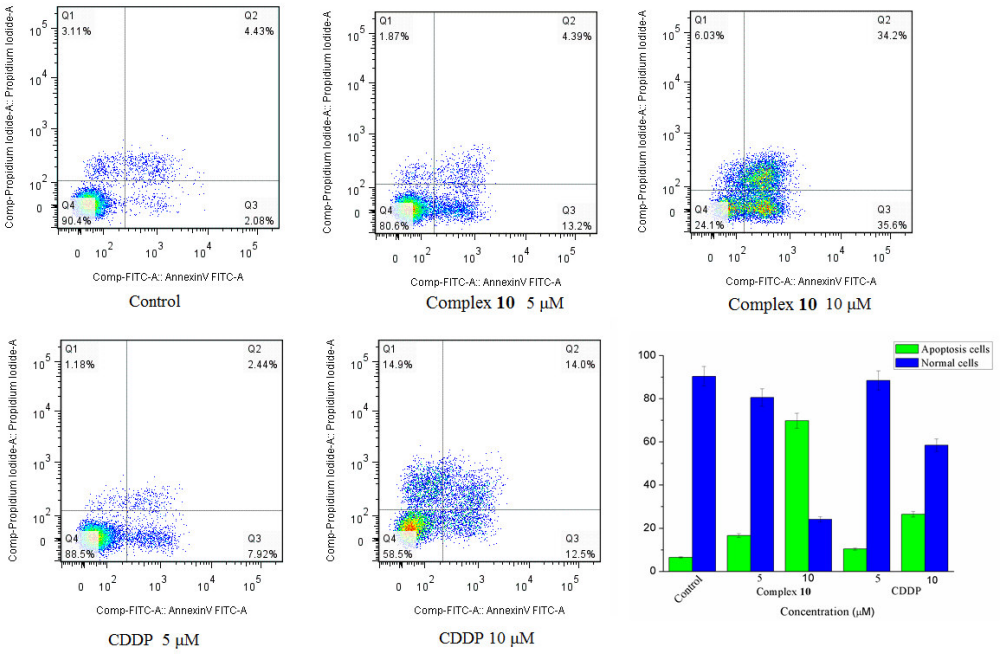

Fig. 8. Representative flow cytometric histograms of apoptotic NCI-H460 cells after 24 h treatment with complex **10** (5, 10 μM) with cispatin (5, 10 μM) as positive control. The cells were harvested and labeled with annexin-V-FITC and PI, and analyzed by flow cytometry. Data are expressed as the mean ± SEM for three independent experiments.

*2.11. Complex **10** induces mitochondrial membrane Permeability in NCI-H460 cells.*

Mitochondria play a key role in cell apoptosis by changing its intracellular and extracellular membrane permeability and resulting in cytochrome c release and caspases activation.[48, 49] Thus, compound **10** was further examined to check whether it induced an alteration of the mitochondrial transmembrane potential (MMP). NCI-H460 cells were treated with compound **10** (5, 10 μM) for 24 h with cisplatin (5, 10 μM) as a positive control, changes in the mitochondrial membrane potential were monitored using the fluorescent dyes JC-1 as described in materials and methods.[49]

As shown in **Fig. 9**, compound **10** induced a dose concentration-dependent increase in the proportion of cells compared with the control, indicating that compound **10** treatment induced mitochondrial membrane permeability in NCI-H460 cells. These results are direct evidence that mitochondrial function is extremely impaired in complex **10** induced apoptosis in NCI-H460 cells.

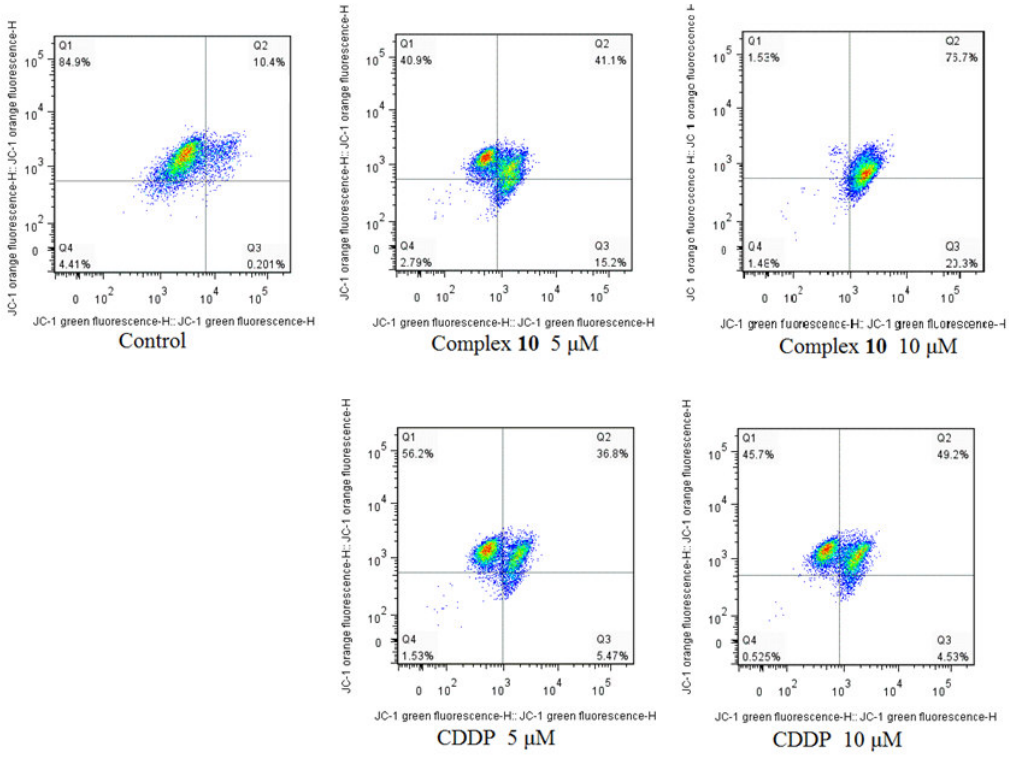

Fig. 9. Assessment of mitochondrial membrane potential (MMP) after treatment of NCI-H460 cells with cisplatin (5, 10 μM) or complex **10** (5, 10 μM). Cells were treated with the indicated concentration of the compound for 24 h and then stained with the fluorescent. Data are expressed as the mean ± SEM of three independent experiments.

*2.12. Complex **10** induces intracellular ROS generation in NCI-H460 cells.*

Mitochondrial membrane depolarization is associated with mitochondrial generation of reactive oxygen species (ROS).[50] ROS production has been implicated as an early event in cell apoptosis. In order to determine whether complex **10** inducing apoptosis is ROS-dependent, NCI-H460 cells were treated with complex **10** (5 and 10 μM) for 24 h and cisplatin (5 and 10 μM) as a positive control, using the fluorescent probe 2,7-dichlorofluorescein diacetate (DCF-DA) by flow cytometry, respectively. As shown in **Fig. 10** A, a good deal of ROS induced by complex **10** was effectively produced compared with control cells, in agreement with the dissipation of the mitochondrial trans-membrane potential. In addition, the effect of complex **10** on the ROS generation was found similar to that of compound **6** as shown in **Fig. 10** A indicating that the ability of complex **10** to generate ROS originated from its precursor (compound **6**). In short, these data indicate that complex **10** induced apoptosis through the mitochondrial pathway.

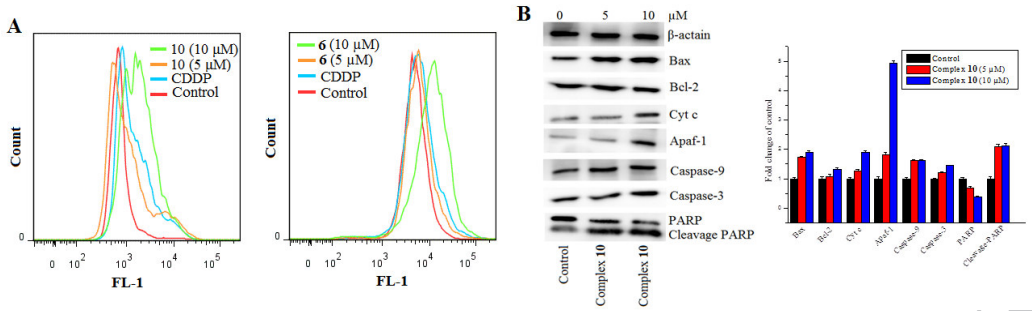

Fig.10. (A) Assessment of the ROS production in NCI-H460 cells. After 24 h incubations with complex **10** and compound **6**, cells were stained with DCF-DA and analyzed by flow cytometry. (B) Western blot analysis of Cyt c, Bax, Bcl-2, Apaf-1, caspase-9, caspase-3 and PARP after treatment of NCI-H460 cells with complex **10** at the indicated concentrations and for the indicated times. β-actin antibody was used as reference control.Data are expressed as the mean ± SEM of three independent experiments.

*2.13. Complex **10** induced apoptosis via the regulation of apoptosis-related protein expression.*

Activation of apoptotic pathways is a major way by which antitumor agents kill tumor cells.[51] It was reported that anticancer drugs can stimulate apoptotic signaling through two major pathways. One is via the extrinsic pathway involved in death receptor and death ligand interaction including Fas receptor and other members of the tumor-necrosis factor (TNF) receptor family; the other is via the intrinsic (mitochondrial) pathway involved in changing the ratio of Bcl-2 family protein, causing loss of mitochondrial membrane integrity and the release of cytochrome c in cytosol, leading to the activation of the caspase cascade and the induction of apoptotic cell death.[52-54] So, the mechanism of action of the newly synthesized complex was further investigated. The mitochondrial related apoptotic proteins of cytochrome c, Bax, Bcl-2, Apaf-1, caspase-9, caspase-3 and PARP were tested in NCI-H460 cells treated with complex **10** (5 and 10 μM) for 48 h using the western blot method. Apoptosis associated protein levels are shown in **Fig. 10** B, which indicated that complex **10** significantly promoted expression of Bax, cytochrome c, Apaf-1, caspase-9, caspase-3 and cleavage-PARP, but reduced levels of Bcl-2 protein that could contribute to cell apoptosis. The above results displayed that the complex **10** inducing apoptotic cell death in NCI-H460 cells occurs via an intrinsic signaling pathway.

*2.14. Anti-tumor effect of complex **10** in vivo.*

To further investigate the antitumor activity of complex **10**, the NCI-H460 tumor xenograft

nude mice were used. As shown in **Fig. 11**, complex **10** inhibited tumor growth in the NCI-H460 tumor xenograft at a dose-dependent manner, and the tumor inhibitory rates on day 28 after treatment were 52.11% and 60.23%, comparable to that of cisplatin, after iv administration at 5 mg/kg (equal weighting dose to cisplatin) and 12 mg/kg (equal molar dose to cisplatin), respectively. Interestingly, complex **10** exhibited a little lower toxicity than cisplatin as time passed, which was evidenced by changes in the weight of the mice after iv administration at 5 mg/kg or 12 mg/kg of complex **10** in the fourth week. The results proved that complex **10** displayed potent anticancer activity which was comparable to that of cisplatin with the equal molar dosage without obvious toxicity *in vivo*, indicating that it might be used as a drug candidate for further research on the therapy of lung carcinoma.

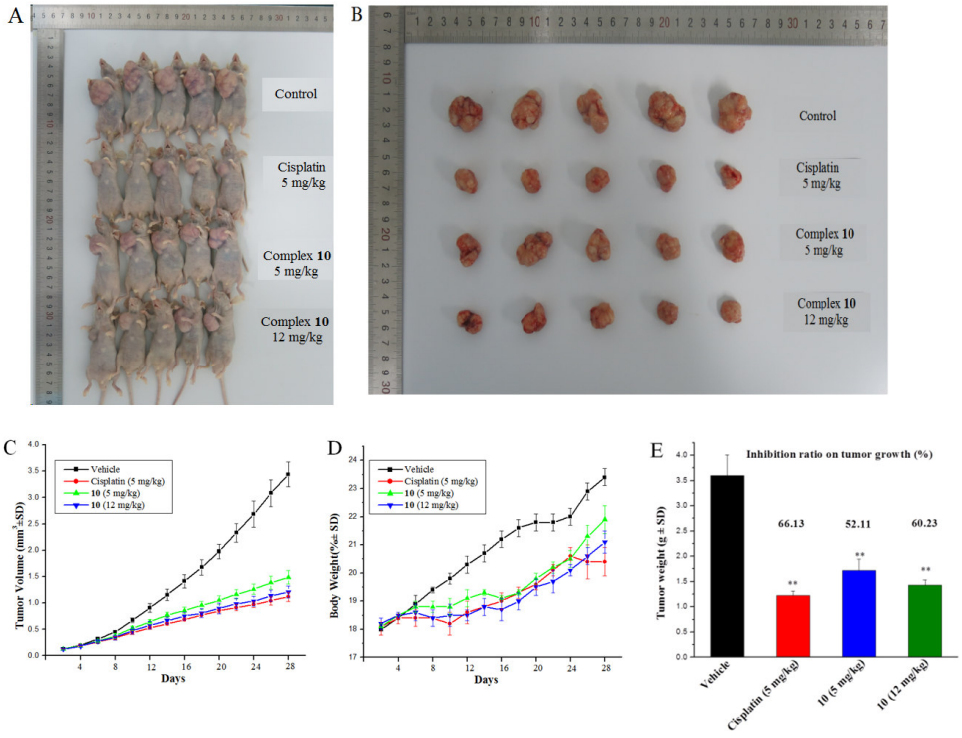

Fig. 11. *In vivo* antitumor activity of complex **10** in mice (BALB/c nude mice) bearing NCI-H460 xenograft. (A-B) After administered with complex **10** at the dose of 5 and 12 mg/kg i.v. once a week for 28 days, cisplatin at the dose of 5 mg/kg for i.v. once a week for 28 days, the mice were sacrificed and weighed the tumors. (C) The tumor volume of the mice in each group during the observation period. (D) The body weight of the mice from each group at the end of the observation period. (E) The weight of the excised tumors of each group. The data were presented

as the mean ± SEM. *P < 0.05.

3. Conclusion

In this investigation, three Pt(IV) prodrugs derived cisplatin, oxaliplatin and DACHPt, containing a phenstatin analogue as a potent inhibitor of tubulin, were designed and synthesized. All resulting Pt(IV) complexes not only exhibited better antitumor activities than their Pt(II) counterparts against the tested cancer cell lines including cisplatin resistant ones, but also displayed less toxic than all the corresponding Pt(II) complexes against two normal human cell lines. Further mechanistic evaluation on complex **10** revealed that it can effectively enter cells, strongly inhibit tubulin polymerization, arrest the cell cycle at G2/M phases, and markedly enhance the cell apoptosis level. More importantly, complex **10** displayed potent activity against SK-OV-3 and A549 cancer cell lines that were resistant to cisplatin, and the resistance index of complex **10** was much lower than cisplatin. Molecular mechanism studies showed that complex **10** caused apoptotic cell death of human non-small lung cancer cell line NCI-H460 through the mitochondrial mediated pathway by releasing mitochondrial cytochrome c, activating Apaf-1, down-regulating Bcl-2, up-regulating Bax, which in turn proteolytically activated downstream caspase-9, caspase-3, and PARP cleavage. It is proved that complex **10** had a potent inhibitory effect on tumor growth in the NCI-H460 xenograft mouse model *in vivo*. Our study suggested that Pt(IV) anticancer prodrugs containing a small molecule fragment that can stimulate or inhibit tubulin polymerization may be a promising approach for multiple targeted cancer therapy.

4. Experimental section

All chemicals and solvents were of analytical reagent grade and provided by Energy Chemical, Shanghai of China and used without further purification, unless noted specifically. Compounds **7-9** were prepared as described previously. [42] The purity of all target compounds used in the biophysical and biological studies was ≥95%. Column chromatography was performed using silica gel (200–300 mesh). The Acitn, Bax, Bcl-2, cytochrome c, caspase-9, caspase-3, Apaf-1, cyclin B1, CDK1, p21 and p53 antibodies were purchased from Imgenex, USA. All tumor cell lines were obtained from the Shanghai Institute for Biological Science (China). ^{1}H NMR and ^{13}C NMR spectra were recorded in $CDCl_3$ or *d6*-DMSO with a Bruker 300 or 400 MHz spectrometer and ^{195}Pt NMR spectra were recorded in *d6*-DMSO with a Bruker 600 spectrometer. Mass spectra were measured on an Agilent 6224 TOF LC/MS instrument. Elemental analyses of C, H, and N used a

Vario MICRO CHNOS elemental analyzer (Elementary).

4.1 General procedure for the preparation of target compounds.

Synthesis of compounds **1-6** and target complexes **10-12**.

Synthesis of compound **1**. To a solution of 3-hydroxy-4-methoxybenzaldehyde (1.52 g, 10.0 mmol) and Et_3N (2.02 g, 20.0 mmol) in dry CH_2Cl_2 (25 mL) was added TBDMSCl (2.25 g, 15.0 mmol) in reaction at 0 °C and the mixture was stirred at room temperature for 2 h. After completion of reaction, the reaction mixture was poured into ice water (150 mL) and extracted with CH_2Cl_2 (2×100 mL). The combined organic phase was washed with saturated NaCl solution, dried over anhydrous Na_2SO_4 and concentrated under reduced pressure to give the desired product as yellow oil (2.5 g, yield 94%) which was used directly without further purification. ^{1}H NMR (300 MHz, $CDCl_3$) δ 9.81 (s, 1H), 7.48 – 7.45 (m, 1H), 7.36 (d, J = 1.7 Hz, 1H), 6.95 (d, J = 8.3 Hz, 1H), 3.88 (s, 3H, -OCH_3), 1.00 (s, 9H, 3×-CH_3), 0.17 (s, 6H, 2×-CH_3). HR-MS (m/z) (ESI): calcd for $C_{14}H_{22}O_3Si$ [M+H^+]: 267.1417; found: 267.1423. Elem Anal. Calcd (%) for C, 62.88; H, 8.67; found: C, 62.60; H, 8.52.

Synthesis of compound **2**. Bromo-3,4,5-trimethoxybenzene (2.47g, 10 mmol）in three-necked round bottomed flask was added dry THF (30 mL) and cooled to -78℃ with a dry ice-acetone bath under a steady stream of dry N_2 gas. Then, 8.3 mL of 1.6 M n-BuLi in hexanes was slowly added into the reaction and the reaction mixture was stirred at the same temperature for 2 h. After for 2 h, the compound **1** (3.2 g, 12 mmol）in dry THF (15 mL) was added to dropwise in portions and the mixture was stirred at room temperature for overnight. TLC showed the reaction was complete. The reaction mixture was poured in ice water (100 mL) and extracted with CH_2Cl_2 (2×100 mL). The organic phase was dried over anhydrous Na_2SO_4 and concentrated under reduce pressure. The residue was purified by silica gel column chromatography eluted with petroleum ether/ethyl acetate to give the desired product (1.5 g, 35%) as a yellow oil. ^{1}H NMR (300 MHz, $CDCl_3$) δ 6.92 – 6.89 (m, 1H), 6.86 (d, J = 1.9 Hz, 1H), 6.81 (d, J = 8.2 Hz, 1H), 6.59 (s, 2H), 5.68 (s, 1H), 3.82 (s, 9H, 2×-OCH_3), 3.79 (s, 3H, -OCH_3), 2.14 (d, J = 16.5 Hz, 1H), 0.97 (s, 9H, 3×-CH_3), 0.13 (s, 6H, 2×-CH_3). HR-MS (m/z) (ESI): calcd for $C_{23}H_{34}O_6Si$ [M+Na^+]: 457.2022; found: 457.2029. Elem Anal. Calcd (%) for C, 63.56; H, 7.89; found: C, 63.42; H, 7.73.

Synthesis of compound **3**. To a solution of compound **2** (1.3 g, 3.0 mmol) in dry DCM (30 mL) was added compound PDC (2.3 g, 6.0 mmol) in portions and the reaction mixture was stirred at

room temperature for overnight. TLC showed the reaction was complete. After completion of reaction, the solid was removed by filtration and the solution was added water (50 mL) and extracted with CH_2Cl_2 (100 mL). The organic phase was dried over anhydrous Na_2SO_4 and concentrated under reduce pressure. The residue was purified by silica gel column chromatography eluted with petroleum ether/ethyl acetate to give the desired product (1.0 g, 83%) as a yellow oil. ^{1}H NMR (300 MHz, $CDCl_3$) δ 7.46 – 7.42 (m, 1H), 7.37 (d, *J* = 1.7 Hz, 1H), 7.02 (s, 2H), 6.90 (d, *J* = 8.4 Hz, 1H), 3.93 (s, 3H, -OCH_3), 3.89 (s, 3H, -OCH_3), 3.88 (s, 6H, 2×-OCH_3), 1.00 (s, 9H, 3×-CH_3), 0.18 (s, 6H, 2×-CH_3). HR-MS (m/z) (ESI): calcd for $C_{23}H_{32}NaO_6Si$ [M+H^+]: 433.2046; found: 433.2053. Elem Anal. Calcd (%) for C, 63.86; H, 7.46; found: C, 63.63; H, 7.22.

Synthesis of compound **4**. To a solution of compound **3** (1.2 g, 2.78 mmol) in dry MeOH (20 mL), 1N MeOH/HCl (8 mL) was added. The reaction mixture was stirred at 50 °C for 2 h, and then cooled to the room temperature. After the solvent was removed by evaporation, the resulting residue was diluted with water (50 mL) and extracted with CH_2Cl_2 (100 mL). The organic phase was dried over anhydrous Na_2SO_4 and concentrated under vacuum. The residue was purified on a silica gel column eluted with petroleum ether/ethyl acetate to give the desired product (850 mg, yield 96.2%) as a white solid. ^{1}H NMR (300 MHz, $CDCl_3$): ^{1}H NMR (300 MHz, CDCl3) δ 7.44 (d, *J* = 1.9 Hz, 1H), 7.41 – 7.38 (m, 1H), 7.03 (s, 2H), 6.93 (d, J = 8.3 Hz, 1H), 5.69 (s, 1H, -OH), 3.99 (s, 3H, -OCH_3), 3.93 (s, 3H, -OCH_3), 3.88 (s, 6H, 2×-OCH_3). HR-MS (m/z) (ESI): calcd for $C_{17}H_{19}O_6$ [M+ H^+]: 319.1182, found: 319.1196. Elem Anal. Calcd (%) for C, 64.14; H, 5.70; found: C, 64.01; H, 5.86.

Synthesis of compound **5**. To a solution of compound **4** (800 mg, 2.52 mmol) in DMF (10 mL), α-bromoethyl acetate (546 mg, 3.27 mmol), K_2CO_3 (695 mg, 5.03 mmol) and KI (42 mg, 0.252 mmol) were added in portions. The mixture reaction was stirred at room temperature for overnight and the reaction was monitored by TLC. After completion of reaction, the mixture was diluted with water (200 mL) and extracted with CH_2Cl_2 (2×100 mL). The organic phase was dried over anhydrous Na_2SO_4 and concentrated under reduced pressure. The residue was purified on silica gel column eluted with petroleum ether/ethyl acetate to give the desired product (1.0 g, yield 98%) as a yellow oil. ^{1}H NMR (300 MHz, $CDCl_3$) δ 7.49 – 7.46 (m, 1H), 7.32 (d, *J* = 6.9 Hz, 1H), 7.00 (s, 2H), 6.95 (d, *J* = 8.4 Hz, 1H), 4.73 (s, 2H), 4.28 – 4.21 (m, 2H), 3.97 (s, 3H, -OCH_3), 3.92 (s, 3H,

-OCH_3), 3.88 (s, 6H, 2×-OCH_3), 1.27 (t, J = 7.1 Hz, 3H, -CH_3). HR-MS (m/z) (ESI): calcd for $C_{21}H_{24}O_8$ [M+H^+]: 405.1549, found: 405.1542. Elem Anal. Calcd (%) for C, 62.37; H, 5.98; found: C, 62.13; H, 6.21.

Synthesis of compound **6**. To a solution of compound **5** (900 mg, 2.23 mmol) in THF (15 mL) lithium hydroxide (280 mg, 6.69 mmol) was added and stirred at room temperature for 2 h. The reaction mixture was adjusted pH = 2 with 1 N HCl solution, the mixture was added water (50 mL) and extracted with CH_2Cl_2 (100 mL), then the organic phase was dried over anhydrous Na_2SO_4 and concentrated under reduced pressure to give the target product (800 mg, yield 95%) as a white solid. ^{1}H NMR (300 MHz, $CDCl_3$): δ 7.51 – 7.48 (m, 1H), 7.44 (d, J = 1.6 Hz, 1H), 7.00 (s, 2H), 6.96 (d, J = 8.4 Hz, 1H), 4.78 (s, 2H), 3.98 (s, 3H, -OCH_3), 3.93 (s, 3H, -OCH_3), 3.87 (s, 6H, 2×-OCH_3). HR-MS (m/z) (ESI): calcd for $C_{19}H_{20}O_8$ [M+H^+]: 377.1236, found: 377.1243. Elem Anal. Calcd (%) for C, 60.64; H, 5.36; found: C, 60.51; H, 5.18.

Synthesis of complexes **10-12**. To a solution of compound **6** (150 mg, 0.399 mmol), TBTU (192 mg, 0.599 mmol) and Et_3N (60 mg, 0.599 mmol) in dry DMF (4 mL), compound **10, 11 or 12** (0.399 mmol) was added in reacion. The mixture was stirred at room temperature for overnight. After completion of reaction, the whole mixture was added CH_2Cl_2 (150 mL), then extracted two times with water (150 mL). The organic phase was dried over anhydrous Na_2SO_4 and concentrated under reduced pressure. The residue was purified on silica gel column eluted CH_2Cl_2/ CH_3OH (40:1) to give the desired product as a yellow solid.

Compound **10**. Yield: 46%. ^{1}H NMR (400 MHz, DMSO-d6) δ 7.38 – 7.36 (m, 2H), 7.10 (d, J = 8.9 Hz, 1H), 6.99 (s, 2H), 6.42 – 5.97 (m, 6H), 4.68 (s, 2H), 3.87 (s, 3H, -OCH_3), 3.81 (s, 6H, 2×-OCH_3), 3.77 (s, 3H, -OCH_3). ^{13}C NMR (100 MHz, DMSO-*d6*) δ 193.7, 175.9, 153.4, 153.0, 147.8, 141.5, 133.2, 123.0, 125.6, 115.1, 111.6, 107.6, 66.7, 60.6, 56.5, 56.3. ^{195}Pt NMR (129 MHz, DMSO-d_6) δ 540.6. HR-MS (m/z) (ESI): calcd for $C_{19}H_{25}Cl_3N_2O_8Pt$ [M+H^+]: 710.0402, found: 710.0417. Elem Anal. Calcd (%) for C, 32.10; H, 3.55; N, 3.94; found: C, 32.01; H, 3.33; N, 3.62.

Compound **11**. Yield: 66%. ^{1}H NMR (400 MHz, DMSO-d6) δ 8.98 – 8.12 (m, 2H), 7.95 – 7.45 (m, 2H), 7.39 – 7.36 (m, 1H), 7.29 (d, J = 1.6 Hz, 1H), 7.10 (d, J = 8.5 Hz, 1H), 6.97 (s, 2H), 4.73 (s, 2H), 3.88 (s, 3H, -OCH_3), 3.81 (s, 6H, 2×-OCH_3), 3.77 (s, 3H, -OCH_3), 2.15 – 2.03 (m, 2H), 1.63 – 1.26 (m, 4H), 1.25 – 0.80 (m, 4H). ^{13}C NMR (100 MHz, DMSO-*d6*) δ 193.6, 177.7, 153.2,

153.0, 147.6, 141.5, 133.2, 129.9, 125.6, 114.3, 111.5, 107.6, 66.9, 63.9, 62.9, 60.6, 56.5, 56.3, 31.4, 31.2, 24.0, 23.8. ^{195}Pt NMR (129 MHz, DMSO-d_6) δ 401.9. HR-MS (m/z) (ESI): calcd for $C_{25}H_{33}Cl_3N_2O_8Pt$ [M+H$^+$]: 790.1028, found: 790.1067. Elem Anal. Calcd (%) for C, 37.96; H, 4.21; N, 3.54; found: C, 37.73; H, 4.34; N, 3.31.

Compound **12**. Yield: 63%. ^{1}H NMR (400 MHz, DMSO-d6) δ 8.37 – 8.27 (m, 2H), 8.00 – 7.95 (m, 2H), 7.67 – 7.24 (m, 1H), 7.37 – 7.35 (m, 1H), 7.08 (d, *J* = 8.5 Hz, 1H), 6.99 (s, 2H), 4.75 (s, 2H), 3.87 (s, 3H), 3.81 (s, 6H), 3.77 (s, 3H), 2.09 – 1.98 (m, 2H), 1.71 – 0.94 (m, 8H). ^{13}C NMR (100 MHz, DMSO-*d6*) δ 193.7, 174.9, 163.6, 163.6, 153.3, 152.9, 147.7, 141.4, 133.3, 129.7, 125.9, 113.7, 111.5, 107.6, 65.4, 62.2, 61.5, 60.6, 56.5, 56.3, 31.3, 31.0, 24.0, 23.9. ^{195}Pt NMR (129 MHz, DMSO-d_6) δ 1014.6. HR-MS (m/z) (ESI): calcd for $C_{25}H_{33}Cl_3N_2O_8Pt$ [M+H$^+$]: 808.1448, found: 808.1483. Elem Anal. Calcd (%) for C, 40.13; H, 4.12; N, 3.47; found: C, 39.90; H, 4.22; N, 3.25.

4.2.The released ability of Pt(IV) complexes under reduction with ascorbic acid.

The released ability of Pt(IV) complexes in a solution of acetonitrile/water (60:40, v:v) was examined by HPLC. The test compounds were made by the addition of ascorbic acid, compound **6**, complexes **10** and **12**, respectively, to a solution containing 60.0% acetonitrile and 40.0% water. The incubation was generated by adding test compounds to a solvent containing 60% acetonitrile and 40% water, which was carried out for 0 h, 1 h and 2 h at 25 °C, respectively. Reversed-phase HPLC was performed with a 250×4.5 mm ODS column. HPLC profiles were recorded on UV detection at 210 nm. Mobile phase comprised of acetonitrile /Water (60:40, v/v), and flow rate was 1.0 mL/min. The samples were taken for HPLC analysis after filtered by 0.45 μm filter.

4.3. Cell culture and maintenance.

All cancer cell lines and two human normal cell lines in this study were purchased from China Life Science Collage (Shanghai, PRC). Culture medium Dulbecco's modified Eagle medium (DMEM), fetal bovine serum (FBS), phosphate buffered saline (PBS, pH = 7.2), and Antibiotice-Antimycotic came from KeyGen Biotech Company (China). Cell lines were grown in the supplemented with 10% FBS, 100 units/ml of penicillin and 100 g/ml of streptomycin in a humidified atmosphere of 5% CO_2 at 37 ^{o}C.

4.4 Cytotoxicity assay (MTT).

The antitumor activity of the target compounds (**6**, **10-12**) as well as the positive drugs were

dissolved in DMF and evaluated in five human cancer cell lines (HepG-2, Bel-7404, NCI-H460, MGC-803 and A549), two human normal cell lines (NCM460 and HL-7702) and two cisplatin resistant cell lines (SK-OV-3/CDDP and A549/CDDP), respectively. About 5×10^4 cells/mL cells, which were in the logarithmic phase, were seeded in each well of 96-well plates and incubated for 12 h at 37 °C in 5% CO_2. Complexes at five different concentrations (2.5, 5, 10, 20 and 50 μM) were then added to the test well and the cells were incubated at 37 °C in a 5% CO_2 atmosphere for 72 h. An enzyme labeling instrument was used to read absorbance with 570/630 nm double wavelength measurement. Cytotoxicity was examined on the percentage of cell survival compared with the negative control. The final IC_{50} values were calculated by the Bliss method (n = 5). All of the tests were repeated in triplicate.

4.5. Cellular uptake test.

NCI-H460 cells were seeded in each well of 96-well plates. After the cells reached about 80% confluence, NCI-H460 cells were treated with different concentrations of the test complex **10** for 24 h, respectively**.** After completion of 12 h incubation, cells were collected and washed three times with ice-cold PBS, then centrifuged at 1000×g for 10 min and resuspended in 1 mL PBS. A volume of 100 μL was taken out to examine the cell density. The remaining cells were digested by HNO_3 (200 μL, 65%) at 65 ^oC for 12 h. The Pt level in cells were examined by ICP-MS.

4.6. Tubulin polymerization assay in vitro and competitive inhibition assays.

Tubulin polymerization assay was monitored by the change in optical density at 340 nm using a modification of methods described by Jordan et al.[55] Purified brain tubulin polymerization kit was purchased from Cytoskeleton (BK006P, Denver, CO). The final buffer concentrations for tubulin polymerization contained 80.0 mM piperazine-N,N′-bis(2-ethanesulfonic acid)sequisodium salt (pH 6.9), 2.0 mM $MgCl_2$, 0.5 mM ethylene glycol bis(β-aminoethyl ether)-N,N,N′,N′-tetraacetic acid (EGTA), 1 mM GTP, and 10.2% glycerol. Test compounds were added in different concentrations, and then all components except the purified tubulin were warmed to 37 °C. The reaction was initiated by the addition of tubulin to a final concentration of 3.0 mg/mL. Paclitaxel, CA-4 and phenstatin were used as positive controls under the same conditions. The optical density was measured for 1 h at 1 min intervals in BioTek's Synergy 4 multifunction microplate spectrophotometer with a temperature controlled cuvette holder. Assays were performed according to the manufacturer's instructions and under conditions similar to those

employed for the tubulin polymerization assays described above.[56, 57] To further evaluated whether the competitive binding activity of inhibitors was investigated using a [^{3}H] colchicine competition scintillation proximity (SPA) assay.[58] The test compounds were pre-incubated with tubulin in different concentrations (5, 10, 15, 20, and 25 μM, respectively), which used to compete with colchicine originally bound to tubulin. After completion of incubation, the filtrate was obtained as described.[59] The ability of the test compounds to inhibit colchicine binding to tubulin was measured as described previously [60] except that the reaction mixtures contained 1 μM tubulin, 5 μM [^{3} H] colchicine, and 5 μM test compound, respectively.

4.7. Molecular modeling.

All the docking studies were carried out using Sybyl-X 2.0 on a windows workstation. The crystal structure of the tubulin in complex with colchicine was retrieved from the RCSB Protein Data Bank (PDB: 3E22.pdb).[61, 62] The synthetic phenstatin analogues, including the parent compound CA-4 and phenstatin, were selected for the docking studies. The 3D structures of these selected compounds were first built using Sybyl-X 2.0 sketch followed by energy minimization using the MMFF94 force field and Gasteiger-Marsili charges. We employed Powell's method for optimizing the geometry with a distance dependent dielectric constant and a termination energy gradient of 0.005 kcal/mol. All the selected compounds were automatically docked into the colchicine binding pocket of tubulin by an empirical scoring function and a patented search engine in the Surflex docking program. Before the docking process, the natural ligand was extracted; the water molecules were removed from the crystal structure. Subsequently, the protein was prepared by using the Biopolymer module implemented in Sybyl. The polar hydrogen atoms were added. The automated docking manner was applied in the present work. Other parameters were established by default to estimate the binding affinity characterized by the Surflex-Dock scores in the software. Surflex-Dock total scores, which were expressed in -log10 (Kd) units to represent binding affinities, were applied to estimate the ligand-receptor interactions of newly designed molecules. A higher score represents stronger binding affinity. The optimal binding pose of the docked compounds was selected based on the Surflex scores and visual inspection of the docked complexes.

4.8. Flow cytometry analysis of cell cycle distribution.

The NCI-H460 cells were grown on 6-well plates and treated with complex **10** (5, 10 μM) and

CDDP (10 μM) and maintained with of the proper culture medium in 5% CO_2 at 37 °C for 24 h . After completion of incubation, cells were harvested and washed twice with ice-cold PBS, fixed with ice-cold 70% ethanol at -20 °C for overnight. The cells were treated with 100 μg /mL RNase A for 30 minutes at 37 °C after washed with twice ice-cold PBS, and finally stained with 1 mg/ml propidium iodide (PI) in the dark at 4 °C for 1 h. Analysis was performed with the system software (Cell Quest; BD Biosciences).

4.9. Apoptosis analysis.

Apoptosis was examined by flow cytometric analysis of annexin V/PI staining. NCI-H460 cells were seeded in each well of 96-well plates at the density of 1×10^5 cells/mL of the DMEM medium with 10% FBS to the final volume of 2 mL. The plates were incubated for overnight and treated with different concentrations of the test compound **10** and CDDP for 24 h. Briefly, cells were harvested and washed with twice ice-cold PBS, and then suspended cells in the annexin-binding buffer at a concentration of 5×10^5 cells /ml. cells were then incubated with 5 μL of annexin V-FITC and 5 μL of PI for 30 minutes at room temperature in the dark. The cells were analyzed by system software (Cell Quest; BD Biosciences).

4.10. Determination of mitochondrial membrane potential.

The mitochondrial membrane potential was measured with the lipophilic cation probe JC-1 (Beyotime, Haimen, China, Molecular Probe), as previously described.[50] NCI-H460 cells were treated with different concentrations of the test compounds for 24 h. After for 24 h, the JC-1 fluorescent probe was added 20 minutes after replacing with fresh medium. Cells were collected at 2500 rpm and washed twice with ice-cold PBS and mitochondrial membrane potential were analyzed by flow cytometer. The emission fluorescence for JC-1 was monitored at 530 and 590 nm, under the excitation wavelength at 488 nm, respectively.

4.11. ROS assay.

The production of ROS was measured by flow cytometry using DCFH-DA (Molecular Probe, Beyotime, Haimen, China), as previously described.[50] NCI-H460 cells were seeded into six-well plates and subjected to various treatments. On the following treatment, cells were harvested at 2000 rpm and washed twice with ice-cold PBS, and then resuspend cells in 10mM DCFH-DA dissolved in cell free medium at 37 °C for 30 min in dark, and then washed twice with PBS. Cellular fluorescence was evaluated by flow cytometry at an excitation of 485 nm and an emission

of 538 nm.

4.12. Western blot analysis.

Western blot analysis was performed as described previously.[50] NCI-H460 cells were treated with different concentrations of the test complex **10** for 48 h. After for 48 h, cells were collected, centrifuged, and washed twice with ice-cold PBS. The pellet was then resuspended in lysis buffer. After the cells were lysed on ice for 30 min, lysates were centrifuged at 20000g at 4 °C for 10 min. The protein concentration in the supernatant was evaluated using the BCA protein assay reagents (Imgenex, USA). Equal amounts of protein per line were was separated on 12% SDS polyacrylamide gel electrophoresis and transferred to PVDF Hybond-P membrane (GE Healthcare). Membranes were incubated with 5% skim milk in Tris-buffered saline with Tween 20 (TBST) buffer for 1 h and then the membranes being gently rotated overnight at 4 °C. Membranes were then incubated with primary antibodies against Bcl-2, Bax, Apaf-1, Cyt c, PARP, caspase-9, caspase-3, p21, p53, cyclin B 1, CDK1, or β-actin for overnight at 4 °C. Membranes were next incubated with peroxidase labeled secondary antibodies for 2 h. Then all membranes were washed with TBST four times for 20 minutes and the protein blots were examined with chemiluminescence reagent (Thermo Fischer Scientifics Ltd.). The X-ray films were developed with developer and fixed with fixer solution.

4.13. Antitumor activity in vivo.

The *in vivo* antitumor activity of compound **10** was evaluated using a human lung carcinoma cell line NCI-H460 in BALB/c nude mice. Five week-old male BALB/c nude mice were housed purchased from Shanghai Ling Chang biotechnology company (China), tumors were induced by a subcutaneous injection in their dorsal region of 1×10^7 cells in 100 μL of sterile PBS. Animals were casually divided into four groups, and starting on the second day. When the tumors reached a volume of 100–150 mm^3 in all mice on day 15, the first group was injected with an equivalent volume of 5% dextrose injection via a tail vein injection as the vehicle control mice. The second group was treated with cisplatin at the doses of 5 mg/kg body weight once a week for four weeks, respectively. No.3 and No.4 groups were treated with complex **10** at the doses of 5 mg/kg (equal weighting dose to cisplatin) or 12 mg/kg (equal molar dose to cisplatin) body weight once a week for four weeks, respectively. All compounds were dissolved in vehicle. Tumor volume and body weights were recorded every other day after drug treatment. All mice were sacrificed after

four weeks of treatment and the tumor volumes were measured with electronic digital calipers and examined by measuring length (A) and width (B) to calculate volume ($V = AB^2/2$).

4.14. Statistical analysis

All statistical analysis was performed with SPSS Version 10. Data was analyzed by one-way ANOVA. Mean separations were performed using the least significant difference method. Each experiment was replicated thrice, and all experiments yielded similar results. Measurements from all the replicates were combined, and treatment effects were analyzed.

Acknowledgments

We are grateful to the National Natural Science Foundation of China (Grant No. 21571033) and the New Drug Creation Project of the National Science and Technology Major Foundation of China (Grant No. 2015ZX09101032) for financial aids to this work. The authors would also like to thank the Fundamental Research Funds for the Central Universities (Project 2242016K30020) for supplying basic facilities to our key laboratory. We also want to express our gratitude to the Priority Academic Program Development of Jiangsu Higher Education Institutions for the construction of fundamental facilities (Project 1107047002). Huang is grateful to the Innovation Program of Jiangsu Province postgraduate education (Project KYLX16_0263). The research was also supported by the Scientific Research Foundation of Graduated School of Southeast University (YBJJ1677). Jiangsu KeyGen Biotech Company (China) was appreciated for completing the *in vivo* tests.

References

1. Wong E, Giandomenico CM. Current status of platinum-based antitumor drugs. *Chem. Rev.* 1999; 99: 2451-2466.
2. Guo Z, Sadler PJ. Metals in medicine. *Angew. Chem. Int. Ed.* 1999; 38: 1512-1531.
3. Oral AY, Cevatemre B, Sarimahmut M, Icsel C, Yilmaz VT, Ulukay E. Anti-growth effect of a novel trans-dichloridobis[2-(2-hydroxyethyl)pyridine]platinum(II) complex via induction of apoptosis on breast cancer cell lines. *Bioorg. Med. Chem*. 2015; 23: 4303-4310.
4. Xue ZQ, Lin MX, Zhu JH, Zhang JF, Li YZ, Guo Z. J. Platinum(II) compounds bearing bone-targeting group: synthesis, crystal structure and antitumor activity. *Chem. Commun.* 2010; 46: 1212-1214.

5. Qian W, Salamoun J, Wang JN, Roginskaya V, Houten BV, Peter W. The combination of thioxodihydroquinazolinones and platinum drugs reverses platinum resistance in tumor cells by inducing mitochondrial apoptosis independent of Bax and Bak. *Bioorg. Med. Chem*. 2015; 25: 856-863.

6. Zhang HY, Gou SH, Zhao J, Chen FH, Xu G, Liu X. Cytotoxicity profile of novel sterically hindered platinum(II) complexes with (1R, 2R)-N^1, N^2-dibutyl-1, 2-diaminocyclohexane. *Eur. J. Med. Chem.* 2015; 96: 187-195.

7. Chin, CF, Tian Q, Setyawati, MI, Fang W, Tan ESQ, Leong DT, Ang WH. Tuning the activity of platinum(IV) anticancer complexes through asymmetric acylation. *J. Med. Chem.* 2012; 55: 7571-7582.

8. Yu HY, Gou SH, Wang ZM, Chen FH, Fang L. Toward overcoming cisplatin resistance via sterically hindered platinum(II) complexes. *Eur. J. Med. Chem.* 2016; 114: 141-152.

9. Hao T, Chen D, Liu K, Qi Y, Tian Y, Sun P, Liu Y, Li Z. Micelles of d-α-tocopheryl polyethylene glycol 2000 succinate (TPGS 2K) for doxorubicin delivery with reversal of multidrug resistance. *Appl. Mater. Interfaces*. 2015; 7: 18064-18075.

10. Li WL, Jiang M, Cao Y, Yan LS, Qi RG, Li YX, Jing XB. Turning ineffective transplatin into a highly potent anticancer drug via a prodrug strategy for drug delivery and inhibiting cisplatin drug resistance. *Bioconjugate Chem*. 2016; 27: 1802-1806.

11. Fang L, Feng MC, Chen FH, Liu X, Shen H, Zhao J, Gou SH. Oleanolic acid-NO donor-platinum(II) trihybrid molecules: Targeting cytotoxicity on hepatoma cells with combined action mode and good safety. *Bioorg. Med. Chem*. 2016; 24: 4611-4619.

12. Mukherjea D, Rybak LP, Sheehan KE, Kaur T, Ramkumar V, Jajoo S, Sheth S. The design and screening of drugs to prevent acquired sensorineural hearing loss. *Expert. Opin. Drug Saf*. 2011; 6: 491-505.

13. Huang XC, Huang RZ, Li LX, Gou SH, Wang HS. Synthesis and biological evaluation of novel chalcone derivatives as a new class of microtubule destabilizing agents. *Eur. J. Med. Chem.* 2017; 132: 11-25.

14. Phoa AF, Browne S, Gurgis FMS, Åkerfeldt MC, Döbber A, Renn C, Peifer C, Stringer BW, et al. Pharmacology of novel small-molecule tubulin inhibitors in glioblastoma cells with enhanced EGFR signaling. *Biochem. Pharmacol*. 2015; 98: 587-601.

15. Kavallaris M. Microtubules and resistance to tubulin-binding agents. *Nat. Rev. Cancer*. 2010; 10: 194-204.

16. Heald R, Nogales E. Microtubule dynamics. *J. Cell Sci.* 2002; 115: 3-4.

17. McIntosh JR, Grishchuk E, West RR. Chromosome-microtubule interactions during mitosis. *Annu. Rev. Cell Dev. Biol.* 2002; 18: 193-219.

18. Cao D, Han XL, Wang GC, Yang Z, Peng F, Ma L, Zhang RH, Ye HY, Tang MH. et al. Synthesis and biological evaluation of novel pyranochalcone derivatives as a new class of microtubule stabilizing agents. *Eur. J. Med. Chem*. 2013; 62: 579-589.

19. Kamal A, Shaik AB, Polepalli S, Kumar GB, Reddy VS, Mahesh R, Garimella S, Jain N. Synthesis of arylpyrazole linked benzimidazole conjugates as potential microtubule disruptors. *Bioorg. Med. Chem*. 2015; 23: 1082-1095.

20. Chen H, Li YM, Sheng CQ, Lv ZL, Dong GQ, Wang TT, Liu J, Zhang MF, Li LZ. et al. Design and synthesis of cyclopropylamide analogues of combretastatin-A4 as novel microtubule-stabilizing agents. *J. Med. Chem.* 2013; 56: 685-699.

21. Pettit GR, Cragg GM, Herald DL, Schmidt JM, Lohavanijaya P. Isolation and structure of combretastatin. *Can. J. Chem.* 1982; 60: 1374-1376.

22. Romagnoli R, Baraldi PG, Salvador MK, Prencipe F, Cara CL, Ortega SS, Brancale A, Hamel E, Castagliuolo I, Mitola S. Design, synthesis, in vitro, and in vivo anticancer and anti-angiogenic activity of novel 3-arylaminobenzofuran derivatives targeting the colchicine site on tubulin. *J. Med. Chem.* 2015; 58: 3209-3222.

23. McGown AT; Fox BW. Differential cytotoxicity of combretastatins A1 and A4 in two daunobucin-resistant P388 cell lines. *Cancer Chemother. Pharmacol.* 1990; 26: 79-81.

24. Dark GG, Hill SA, Prise VE, Tozer GM, Pettit GR, Chaplin DJ. Combretastatin A-4, an agent that displays potent and selective toxicity toward tumor vasculature. *Cancer Res*. 1997; 57: 1829-1834.

25. Schobert R, Biersack B, Dietrich A, Effenberger K, Knauer S, Mueller T. 4-(3-Halo/amino-4,5-dimethoxyphenyl)-5-aryloxazoles and -N-methylimidazoles that are cytotoxic against combretastatin a resistant tumor cells and vascular disrupting in a cisplatin resistant germ cell tumor model. *J. Med. Chem.* 2010; 53: 6595-6602.

26. Yan J, Pang YQ, Sheng JF, Wang YL, Chen J, Hu JH, Huang L, Li XS. A novel synthetic

compound exerts effective anti-tumor activity in vivo via the inhibition of tubulin polymerisation in A549 Cells. *Biochem. Pharmaco.* 2015; 97: 51-61.

27. Do CV, Faouzi A, Barette C, Farce A, Fauvarque MO, Colomb E, Catry L, Berthier-Vergnes O, Haftek M, Barret R, Lomberget T. Synthesis and biological evaluation of thiophene and benzo[b]thiophene analogs of combretastatin A-4 and isocombretastatin A-4: A comparison between the linkage positions of the 3,4,5-trimethoxystyrene unit. *Bioorg. Med. Chem*. 2016; 26: 174-180.
28. Pettit GR, Rhodes MR, Herald DL, Chaplin DJ, Stratford MR, Hamel E, Pettit RK, Chapuis J C, Oliva D. Synthesis of the trans-isomer of combretastatin A-4 prodrug. *Anticancer Drug Des.* 1998; 13: 981-993.
29. Fura A, Shu YZ, Zhu M, Hanson RL, Roongta V, Humphreys WG. Discovering drugs through biological transformation: role of pharmacologically active metabolites in drug discovery. *J. Med. Chem.* 2004; 47: 4339-4351.
30. Broc-Ryckewaert DL, Pommery N, Pommery J, Ghinet A, Farce A, Wiart JF, Gautret P, Rigo B, Hénichart JP. In vitro metabolism of phenstatin: potential pharmacological consequences. *Drug Metabolism Letters*. 2011; 5: 209-215.
31. Schobert R, Biersack B, Dietrich A, Knauer S, Zoldakova M, Fruehauf A, Mueller T. Pt (II) complexes of a combretastatin A-4 analogous chalcone: effects of conjugation on cytotoxicity, tumor specificity, and long-term tumor growth suppression. *J. Med. Chem.* 2009; 52: 241-246.
32. Yuan Y, Kwok RTK, Tang BZ, Liu B. Targeted theranostic platinum(IV) prodrug with a built-in aggregation-induced emission light-up apoptosis sensor for noninvasive early evaluation of its therapeutic responses in situ. *J. Am. Chem. Soc.* 2014; 136: 2546-2554.
33. Han XP, Sun J, Wang Y J, He ZG. Recent advances in platinum(IV) complex-based delivery systems to improve platinum(II) anticancer therapy. *Med. Res. Re*. 2015; 35: 1268-1299.
34. Ma LL, Ma, R, Wang, YP, Zhu XY, Zhang JL, Chan HC, Chen XF, Zhang WJ, Chiu SK, Zhu GY. Chalcoplatin, a dual-targeting and p53 activator containing anticancer platinum(IV) pro-drug with unique mode of action. *Chem. Commun.* 2015; 51: 6301-6304.
35. Pathak RK, Marrache S, Choi JH, Berding TB, Dhar S. The pro-drug platin-A: simultaneous release of cisplatin and aspirin. *Angew. Chem. Int. Ed.* 2014; 53: 1963-1967.
36. Raveendran R, Braude JP, Wexselblatt E, Novohradsky V, Stuchlikova O, Brabec V, Gandin V,

Gibson D. Pt (IV) derivatives of cisplatin and oxaliplatin with phenylbutyrate axial ligands are potent cytotoxic agents that act by several mechanisms of action. *Chem. Sci*. 2016; 7: 2381-2391.

37. Qin XD, Xu G, Chen FH, Fang L, Gou SH. Novel platinum(IV) complexes conjugated with a wogonin derivative as multi-targeted anticancer agents. *Bioorg. Med. Chem*. 2017; 25: 2507-2517.
38. Xue X, You S, Zhang Q, Wu Y; Zou GZ, Wang PC, Zhao YL, Xu Y, Jia L, Zhang XN. et al. Mitaplatin increases sensitivity of tumor cells to cisplatin by inducing mitochondrial dysfunction. *Mol. Pharmaceutics.* 2012; 9: 634-644.
39. Huang XC, Huang RZ, Gou SH, Wang ZM, Liao ZX, Wang HS. Anticancer platinum(IV) prodrugs containing monoaminophosphonate ester as a targeting group inhibit matrix metalloproteinases and reverse multidrug resistance. *Bioconjugate Chem*. 2017; 28: 1305-1323.
40. Huang XC, Huang RZ, Gou SH, Wang ZM, Liao ZX, Wang HS. Combretastatin A-4 analogue: a dual-targeting and tubulin inhibitor containing antitumor Pt(IV) moiety with a unique mode of action. *Bioconjugate Chem*. 2016; 27: 2132-2148.
41. Chen JH, Brown DP, Wang YJ, Chen ZS. New phenstatin-fatty acid conjugates: synthesis and evaluation. *Bioorg. Med. Chem. Lett*. 2013; 23: 5119-5122.
42. Ravera M, Gabano E, Pelosi G, Fregonese F, Tinello S, Osella D. A new entry to asymmetric platinum(IV) complexes via oxidative chlorination. *Inorg. Chem.* 2014; 53: 9326-9335.
43. Eymin B, Gazzeri S. Role of cell cycle regulators in lung carcinogenesis. *Cell Adh. Migr.* 2010; 4: 114-123.
44. Galimberti F, Thompson, SL, Liu X, Li H, Memoli V, Green SR, DiRenzo J, Greninger P, Sharma SV, Settleman J. et al. Targeting the cyclin E-CDK-2 complex represses lung cancer growth by triggering anaphase Catastrophe. *Clin. Cancer Res.*2010; 16: 109-120.
45. Jackman M, Lindon C, Nigg EA, Pines J. Active cyclin B1-Cdk1 first appears on centrosomes in prophase. *Nat. Cell Biol*. 2003; 5: 143-148.
46. Li Y, Zhang LP, Dai F, Yan WJ, Wang HB, Tu ZS, Zhou B. Hexamethoxylated monocarbonyl analogues of curcumin cause G2/M cell cycle arrest in NCI-H460 cells via michael acceptor dependent redox intervention. *J. Agric. Food Chem*. 2015; 63: 7731-7742.

47. Papazisis KT, Zambouli D, Kimoundri OT, Papadakis ES, Vala V, Geromichalos GD, Voyatzi, S, Markala D, Destouni E, Boutis L. et al. Protein tyrosine kinase inhibitor, genistein, enhances apoptosis and cell cycle arrest in K562 cells treated with γ-irradiation. *Cancer Letters*. 2000; 160: 107-113.

48. Kuwana T, Newmeyer DD. Bcl-2-family proteins and the role of mitochondria in apoptosis. *Curr. Opin. Cell Biol*. 2003; 15: 691-699.

49. Fang ZX, Liao PC, Yang YL, Yang FL, Chen YL, Lam YL, Hua KF, Wu SH. Synthesis and biological evaluation of polyenylpyrrole derivatives as anticancer agents acting through caspases-dependent apoptosis. *J. Med. Chem*. 2010; 53: 7967-7978.

50. Zhang JY, Yi T, Liu J, Zhao Z, Chen HB. Quercetin induces apoptosis via the mitochondrial pathway in KB and KBv200 cells. *J. Agric. Food Chem*. 2013; 61: 2188-2195.

51. Thorburn A. Death receptor-induced cell killing. *Cell. Signalling*. 2004; 16: 139-144.

52. Ashkenazi A, Dixit VM. Apoptosis control by death and decoy receptors. *Curr. Opin. Cell Biol*. 1999; 11: 255-260.

53. Kamachi M, Le TM, Kim SJ, Geiger ME, Anderson P, Utz PJ. Human autoimmune sera as molecular probes for the identification of an autoantigen kinase signaling pathway. *J. Exp. Med.* 2012; 196:1213-1225.

54. Huang SH, Wu LW, Huang AC, Yu CC, Lien JC, Huang YP, Yang JS, Yang JH, Hsiao YP, Wood WG. et al. Benzyl isothiocyanate (BITC) induces G2/M phase arrest and apoptosis in human melanoma A375.S2 cells through reactive oxygen species (ROS) and both mitochondria-dependent and death receptor-mediated multiple signaling pathways. *J. Agric. Food Chem*. 2012; 60: 665-675.

55. Jordan MA, Wilson L. Microtubules as a target for anticancer drugs. *Nat. Rev. Cancer*. 2004; 4: 253-265.

56. Schiff PB, Fant J, Horwitz SB. Promotion of microtubule assembly in vitro by paclitaxel. *Nature.* 1979; 227: 665-667.

57. Schofield AV, Gamell C, Suryadinata R, Sarcevic B, Bernard O. Tubulin polymerization promoting protein 1(Tppp1) phosphorylation by rho-associated coiled-coil kinase(Rock) and cyclin-dependent kinase 1(Cdk1) inhibits microtubule dynamics to increase cell proliferation. *J. Biol. Chem.* 2013; 288: 7907-7917.

58. Liu YN, Wang JJ, Ji YT, Zhao GD, Tang LQ, Zhang CM, Guo XL, Liu ZP. Design, Synthesis, and biological evaluation of 1-Methyl-1,4-dihydroindeno[1,2-c] pyrazole analogues as potential anticancer agents targeting tubulin colchicine binding site. *J. Med. Chem*. 2016; 59: 5341-5355.

59. Li CM, Lu Y, Ahn S, Narayanan R, Miller DD, Dalton JT. Competitive mass spectrometry binding assay for characterization of three binding sites of tubulin. *J. Mass. Spectrom*. 2010; 45: 1160-1166.

60. Verdier-Pinard P, Lai JY, Yoo HD, Yu J, Marquez B, Nagle DG, Nambu M, White JD, Falck JR, Gerwick WH. et al. Structure activity analysis of the interaction of curacin A, the potent colchicines site anti-mitotic agent, with tubulin and effects of analogs on the growth of MCF-7 breast cancer cells. *Mol. Pharmacol*. 1998; 53: 62-67.

61. Wang GC, Peng F, Cao D, Yang Z, Han XL, Liu J, Wu WS, He L, Ma L, Chen JY. et al. Design, synthesis and biological evaluation of millepachine derivatives as a new class of tubulin polymerization inhibitors. *Bioorg. Med. Chem*. 2013; 21: 6844-6854.

62. Yang Z, Wu WS, Wang JJ, Liu L, Li LY, Yang JH, Wang GC, Cao D, Zhang RH, Tang MH. et al. Synthesis and biological evaluation of novel millepachine derivatives as a new class of tubulin polymerization inhibitors. *J. Med. Chem.* 2014; 57: 7977-7989.

Highlights

- Complex **10** exhibited stronger antitumor activity and lower toxicity than cisplatin.
- Complex **10** effectively arrested NCI-H460 cells in G2/M stage.
- Tubulin polymerization assay indicated that **10** could inhibit tubulin polymerization *in vitro*.
- Representative complex **10** may induce apoptosis via two pathways.

Graphical abstract

Platinum(IV) complexes conjugated with phenstatin analogue as inhibitors of microtubule polymerization and reverser of multidrug resistance

Xiaochao Huang, Rizhen Huang, Shaohua Gou, Zhimei Wang, Zhixin Liao and Hengshan Wang